Progress report on the XUV online diagnostic unit for the highly accurate determination of SR properties

Cite as: AIP Conference Proceedings **2054**, 060057 (2019); https://doi.org/10.1063/1.5084688
Published Online: 16 January 2019

Jens Buck, Kai Bagschik, Leif Glaser, Frank Scholz, Jörn Seltmann, and Jens Viefhaus

Progress Report on the XUV Online Diagnostic Unit for the Highly Accurate Determination of SR Properties

Jens Buck[2,3,b)], Kai Bagschik[2], Leif Glaser[2], Frank Scholz[2], Jörn Seltmann[2] and Jens Viefhaus[1,2,a)]

[1]*Helmholtz-Zentrum Berlin für Materialien und Energie GmbH, Germany*
[2]*Deutsches Elektronen-Synchrotron (DESY), Hamburg, Germany*
[3]*IEAP, Christian-Albrechts-Universität zu Kiel, Kiel, Germany*

[a)]Corresponding author: jens.viefhaus@helmholtz-berlin.de
[b)]jens.buck@desy.de

Abstract. Recent results from simultaneous long-term stability measurements of the beam position and photon energy of the synchrotron beam at the soft X-ray beamline P04 at PETRA III (DESY, Hamburg) are presented. The data was obtained by operating the built-in, non-invasive diagnostic unit directly upstream the beamline focus in parallel with a user experiment. We demonstrate that a sophisticated data evaluation based on principal component analysis results a high positional accuracy better than a few micron and a stable photon energy measurement with an uncertainty in the low ppm regime. Even subtle effects caused by abnormalities in the electron storage ring operation (e.g. short interruptions of the electron injection) are revealed hereby. Utilizing online diagnostic data for feedback controls will enable unprecedented stability of beamline operation at synchrotrons and FEL sources in the future.

INTRODUCTION

The XUV Online Diagnostic Unit originally developed for - and integrated into - beamline P04 at PETRA III (DESY, Hamburg) [1] allows to monitor several radiation properties in parallel to a user experiment. The primary application of the method up to date has been the online determination of the polarization and temporal properties of VUV and soft X-ray radiation, predominantly at free electron lasers using a mobile version of the instrument [2–8]. However, the diagnostic unit is also capable of measuring the (relative) mean photon energy as well as the beam position. The measurement principle is based on angle resolved time-of-flight electron spectroscopy employing inert gas phase targets with low partial pressure. Using 16 detectors in a highly redundant geometry, a rather high accuracy for several observables in parallel is achievable.

We will give a short introduction to the device followed by some aspects of data analysis. We will illustrate the capabilities of the device with a special use case at beamline P04 where user-provided experiment setups demand highly stable conditions for extended periods of time to fully benefit from the high energy resolution of the beamline and its microfocus. This is required e.g. during low count rate coincidence measurements [9] of dilute gas phase targets. Here, typically few days of data acquisition have to be combined into one consistent data set. Drifts of the photon energy or the spatial overlap of the SR beam with the gas jet may render the data analysis rather complicated.

APPARATUS AND METHOD

Figure 1(a) shows schematically the arrangement of the experiment setup. The 16 electron time-of-flight spectrometers are situated in a plane perpendicular to the radiation under test. In the interaction region close to the center an inert gas target (mainly rare gases or nitrogen) is injected via a thin capillary. Typical operating chamber pressures are in the range of 10^{-6} hPa. The effective target pressure in the interaction region is about 1-2 orders higher and a base pressure about 3 orders lower than the operating pressure is typically achieved. All spectrometers have their individual entrance

Proceedings of the 13th International Conference on Synchrotron Radiation Instrumentation – SRI2018
AIP Conf. Proc. 2054, 060057-1–060057-7; https://doi.org/10.1063/1.5084688
Published by AIP Publishing. 978-0-7354-1782-3/$30.00

apertures and are well shielded from each other, so individual retarding potentials can be applied to the four isolated flight tube sections of each electron analyzer.

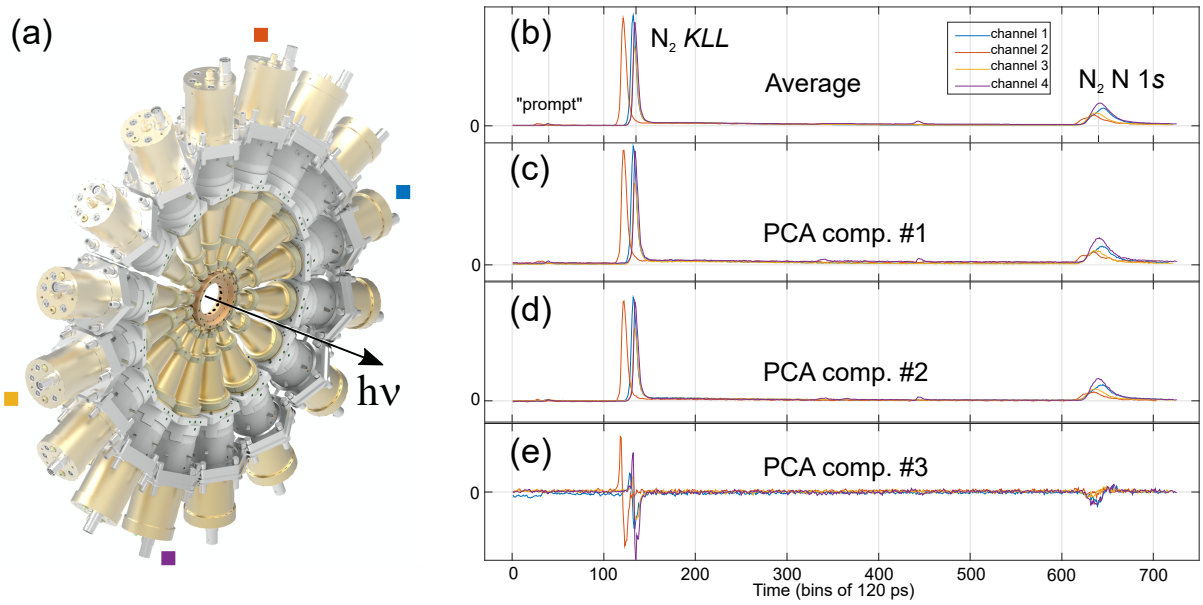

FIGURE 1. (a) Schematic drawing of the online diagnostic unit. The plane spanned by the 16 electron time-of-flight spectrometers is aligned in normal to the radiation under test. Colored squares indicate the two pairs of opposing spectrometers which have been included in the data analysis. (b) Four electron time-of-flight spectra of molecular nitrogen ionized with a photon energy of $h\nu$ = 425 eV. The spectra are the average of a series of spectra. The faster Auger electrons are responsible for the lines marked with N_2 *KLL* on the left hand side, whereas the slower N_2 1*s* photoelectrons are found on the right hand side. The fastest feature marked "prompt" is due to light scattering and fluorescence of the gaseous nitrogen target. (c)-(e) Depict the first three basis vectors resulting from the principal components analysis (see text).

The electrons are registered by multi-channel-plate (MCP) detectors mounted on modified hex-cut CF40-feedthrough-flanges. All detectors are equipped with three MCPs in a Z-stack configuration. Each MCP detector voltage can be adjusted for optimum detector response (typically less than 3kV across all three MCPs). In this design, a FWHM spike width below 1 ns with amplitudes in the order of 10 mV are achieved in the capacitively decoupled and pre-amplifed (> x15) signal output. Two general variants of data acquisition electronics (DAQ) have been used in past experiments: For free electron laser applications, a fast digitizer system (≥ 2 GS/s) is mandatory. In the presented case utilizing synchrotron radiation, the consequently much lower pulse intensity mandates constant fraction discriminators together with a time-to-digital converter (120 ps bins). Here, the flight time of each detected electron is histogrammed, resulting in 16 electron time-of-flight spectra. The duration to reach meaningful statistics depends strongly on the conditions, but the high flux of P04 allows for typical acquisition times as low as a few seconds. In this study, a continuous series of spectra with an acquisition time of 13 s was acquired over a period of ≈2 days. Figure 1(b) shows the average of all spectra from the four relevant detectors.

The results presented here are derived from the analysis of the electron time-of-flight data by means of principal component analysis (PCA) [10] as was proposed earlier for the diagnostic PES device at the European XFEL [11]. The same approach has been further developed and applied to free electron laser data obtained at FLASH2 (DESY, Hamburg) [12]. The PCA is used to map the obtained set of electron spectra into a lower-dimensional, orthogonal basis with uncorrelated components. Figure 1(c)-(e) show the first three basis vectors representing the highest variance. In order to obtain a measure how many basis vectors are required to meaningfully represent the data set, the variance per basis vector in descending order is analysed, see fig. 2(a). Components ≥ 4 reveal close-to-identical variance and no temporal structure, i.e. effectively white noise (e. g. bottom graph of basis vector #4 in fig. 2(b)), but the coefficients of the first three basis vectors show strongly systematic variations with time. We can thus safely assume that the vital information of the dynamics of the system is represented by only the first three PCA components.

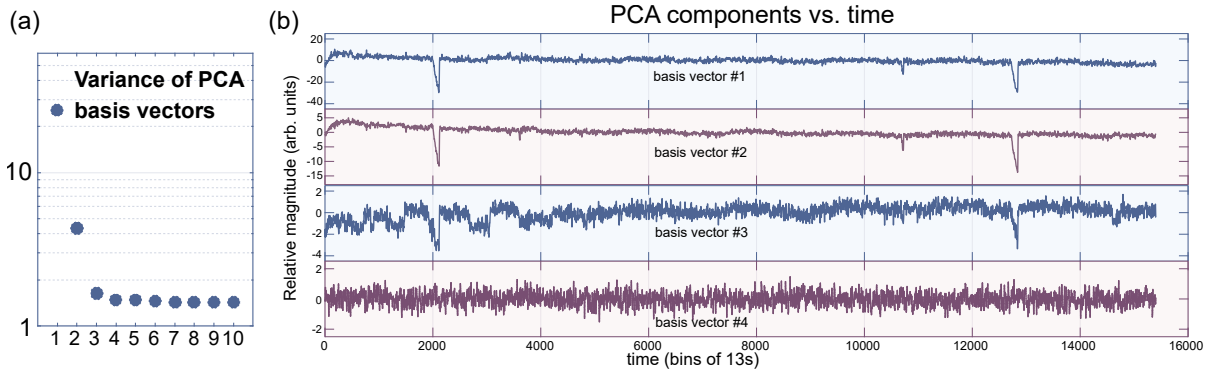

FIGURE 2. (a) Variance per basis vector, indicating that most of the variance in the data is contained already in the first three basis vectors. (b) Time series of the coefficients of the four basis vectors utilized to represent the complete set of electron spectra.

RESULTS

Like all modern third-generation synchrotron facilities, PETRA III is running in a so-called top-up-injection mode where the inevitable loss of circulating electron current is compensated by frequent injections in order to maintain a nearly constant synchrotron radiation intensity. In the present case this "top-up" was interrupted during the sequence of the measurements due to technical issues in the pre-accelerator chain. Therefore the PETRA III ring current depicted in fig. 3(a) shows a few "dips".

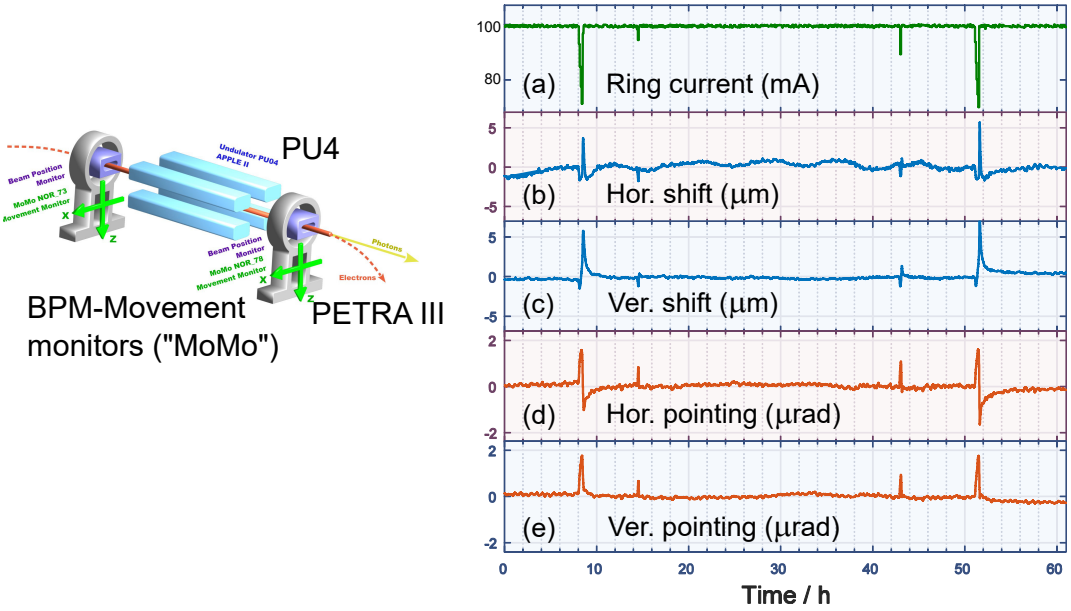

FIGURE 3. (a) Electron current in the PETRA III storage ring during the measurement campaign. The partial loss of current is due to technical issues of the pre-accelerator chain. (b)-(e) Derived quantities from the movement monitors of the beam position monitors situated in the vicinity of the undulator radiation source: (b),(c) Effective horizontal and vertical shift of the source point, respectively. (d),(e) Effective deviation of the horizontal and vertical angular direction of the radiation, respectively.

While the direct consequence of a partial loss of the beam current (here <20%), a reduced photon flux, can usually be eliminated from experimental data by intensity normalization using the beam current, the changed heat load on all components of the storage ring and the beamline exposed to radiation will cause a highly non-trivial response. At PETRA III, the specific influence on the placement of the beam position monitors, situated before and

after every undulator, is routinely monitored using so-called movement monitors ("MoMo"). Figure 3(b)-(e) shows the derived quantities based on the "MoMo"-data. The recorded movement of the two beam position monitors in question has been used to approximately calculate the deviations of the synchrotron radiation source position and its angular direction (pointing). It is clearly visible that even the short "top-up" interruptions have been causing a disturbance of the source, although its magnitude is still quite small, keeping in mind that the effective source size is about 300 μm by 10 μm (FWHM) in the horizontal and vertical direction, respectively.

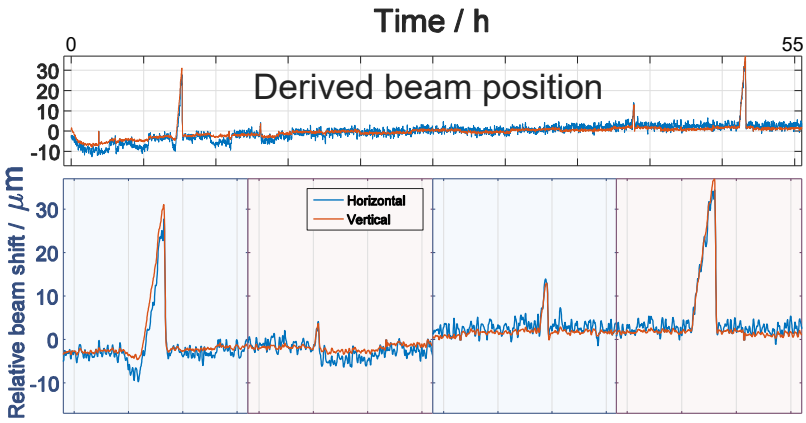

FIGURE 4. Time series of beam position displacements at the diagnostic unit derived from the measured electron time-of-flight data of the horizontal (blue line) and vertical (red line) analyzer pair, respectively. The bottom part shows four enlarged time intervals where interruptions of the top-up injection occurred.

We can clearly correlate the data from the online diagnostics unit with that from the MoMos and thus understand to what extent small changes in the source propagate through the beamline. Figure 4 shows the calculated beam displacement at the position of the diagnostic unit in the horizontal and vertical plane, respectively. The insets at the bottom zoom into the regions where the "top-up" interruptions occurred.

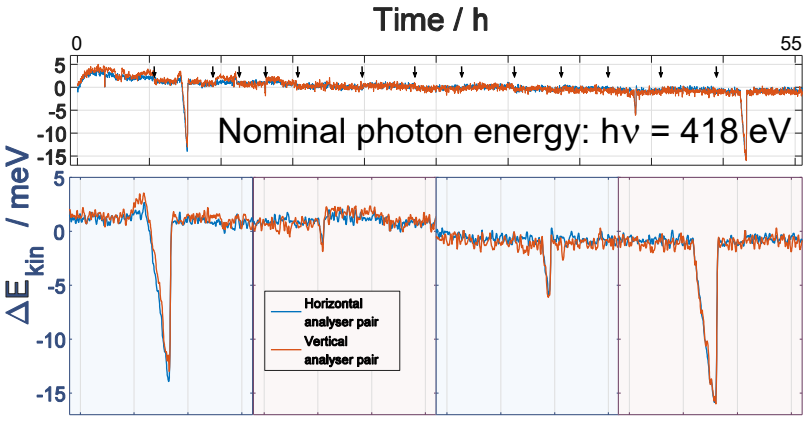

FIGURE 5. Time series of the actual relative photon energy derived from the measured electron time-of-flight data of a horizontal (blue line) and vertical (red line) analyzer pair, respectively. The bottom part shows four enlarged time intervals where interruptions of the top-up injection occurred. Small vertical arrows indicate the time when the magnetic structure of the undulator was changed in order to reverse the helicity of the circularly polarized radiation.

A measured beam displacement at only one point along the beamline does obviously not allow to distinguish both translation and angular deviation unambiguously. However, the diagnostic unit additionally provides a measure of the actual photon energy, making it especially sensitive to pointing variations in the vertical plane (plane of dispersion of the grating monochromator). Nevertheless, a direct quantitative comparison of the data measured with the movement monitors (fig. 3 (b)-(e)) with that derived from the diagnostic unit data (fig. 4 and 5, respectively) would require

additional information. Qualitatively and with respect to the observed order of magnitude, the two data sets are in agreement with each other.

Using the Auger electron lines and the "prompt" signal (see fig. 1 (b)) as a calibration together with the measured photoelectron time-of-flight data, one can derive the relative changes of the photon energy quite accurately. Figure 5 provides a clear signature of changes of the photon energy during the periods when the top-up injection stopped. The agreement of the results obtained independently from both the horizontal and the vertical analyzer pair is remarkable, as the systematic difference found is very close to the noise level. From the beamline operational point of view, the results are quite satisfactory: even in the extreme cases the relative deviation is only about 36 ppm at 418 eV photon energy. Nevertheless, drifts of this magnitude are a significant limiting factor in very sensitive experiments such as circular dichroism measurements. We conclude that its sensitivity qualifies the method to verify future improvements of the beamline.

Pronounced drifts during the first 1-2 hours of operation of the diagnostic unit are a well known feature in our long-term measurements and they are also found in figs. 4 and 5. The reason for this is not yet fully understood. Possible explanations are thermal effects on the beamline optics or effects on the spectrometers due to the permanent injection of the target gas. Further studies are necessary in order to segregate and control these processes. The time periods of stationary operation exhibit further very small, systematic, and step-like variations of the derived photon energy. These coincide with changes of the light's helicity between left and right circular, i.e. when the magnetic field in the APPLE II-type undulator of beamline P04 is altered by suitable shifts of the magnet (half row) structure. The observed magnitude is just outside the noise level (few ppm) here, but small changes of beam pointing are a plausible side effect of changing the undulator shift. This again motivates more systematic studies in order to pin down the root cause of this effect.

As mentioned before, the time evolution found in the presented data set is a combination of the effects from instabilities of the storage ring (e.g., the effect from suspended top-up injection), user operation (small change of pointing from changing helicity), slow drifts of the ring, the beamline, and the spectrometer as well as statistical uncertainty of the measurement. Where the first two items can clearly be correlated with the archived state of the facility, the latter ones are more subtle and cannot easily be disentangled without further references. In order to quantitatively summarize the present findings, we present an assessment of the combined stability and reproducibility of the involved components during the evaluated period. In order to obtain a figure of merit of 'local' stability, we compute a moving standard deviation of all time series from figs. 4 and 5 in an environment of ±25 and ±100 data points, respectively. As the transient features introduced from user operation and beam current were rare throughout the measurement period, it is safe to state the median of the moving standard deviation as a typical value representing the combined errors of alignment and measurement during quasi-stationary operation, i.e. during the absence of otherwise observable changes in the machine and beamline. This number incorporates all of the above mentioned effects, so the value derived here serves as an upper limit for the magnitude of each of the contributions.

TABLE 1. Error margins of the observables 'beam position' and 'mean photon energy'.

	eTOF detectors	**Filtered data** $\Delta t = 6.6 \times 13$ **s***	**Filtered data** $\Delta t = 6.6 \times 13$ **s**†	**Raw data** $\Delta t = 13$ **s***
position resolution/stability	hor. pair	2.1	2.4	6.8
(μm)	ver. pair	0.63	0.72	2.0
energy resolution/stability	hor. pair	0.51	0.59	1.7
(meV)	ver. pair	0.71	0.82	2.3

* moving standard deviation over 50 data points (2σ values).
† moving standard deviation over 200 data points (2σ values).

Table 1 summarizes the error margins of the observables 'beam position' and 'mean photon energy', both raw and post-processed with a binomial filter (width 27 points). As the study has been performed with a native time resolution of 13s per single spectrum and the drifts of the beamline under study are expected on a much longer time scale, eliminating large frequencies from the data by applying a temporal filter will preferably eliminate statistical noise, not true drifts. Note that except for the post-processing, no smoothing is ever applied in the time domain, so the time resolution of the measurement is defined by only the acqusition time of a single spectrum and the rise time of the filter, which amounts to 6.6 data points (10% − 90%) in this case. Assuming white noise from counting statistics, the filter eliminates ≈ 90% of the noise power from the results. The accuracy of the measurements is improved by

roughly a factor 3 by filtering. Furthermore, a general tendency towards larger values for a wider environment is seen for the moving standard deviation which does converge for larger values. This indicates an actual drift in the data, so the statistical contribution is not the limiting factor of the reproducibility. The precision of the position measurement is clearly better for the vertical component in all cases. We attribute this finding to the fact that the diagnostic unit is located about 1.4 m outside the beamline focus, where the beam has a strongly elliptical cross section with its larger principal axis pointing horizontally. The measurement precision of energy reveals a larger uncertainty in vertical direction, even though the discrepancy here is much smaller than for the beam position. Subtle, individual deviations of the detectors may play a crucial role here. Here, the higher noise level can be tracked back mainly to the center of gravity measurement of the photoemission line in one of the involved detectors, which has a slightly larger inelastic background. The entire analysis presented relies on TOF measurements of *KLL* Auger electrons and 1*s* photoelectrons, or, precisely speaking, on the center of gravity of the respective lines. Knowledge of the pulse arrival time is not required here, as only TOF differences enter the equations, which instead result a calculated time zero alongside with kinetic energy and beam position. The stationarity and distribution of the calculated time zero can be compared with the spectroscopic data as a consistency check. In the present case, we obtain distributions with a standard deviation between 1.07 ps and 1.76 ps in every analyser channel (unfiltered data) which is by far smaller than the time resolution of the TDCs.

CONCLUSIONS

We reported on the performance of the diagnostic unit of beamline P04 at PETRA III where the the synchrotron radiation users demanded especially stable conditions for extended periods of time. Processing all available data with a thorough principal components analysis revealed the trends of the parameters of interest. Relative changes of the photon energy could be detected with few ppm accuracy revealing minute changes mostly due to storage ring related events. The simultaneously derived beam position showed corresponding movements in the range of few μm. Such online diagnostic data provides valuable information for the correct interpretation of the user experiments. Ultimately they could also allow to stabilize important radiation properties via suitable feedback systems in real-time for unprecedented beamline stability, an important aspect for future storage ring based synchrotron radiation light sources such as PETRA IV or BESSY III. Furthermore the diagnostic unit presented here is also compatible with high repetition rate X-ray free electron lasers such as the European XFEL or the upcoming LCLS-II.

ACKNOWLEDGMENTS

We acknowledge strong support by the user community of beamline P04 at PETRA III as well as fruitful discussions with Markus Braune and Gregor Hartmann on numerous aspects of electron time-of-flight spectroscopy, diagnostics and data analysis.

REFERENCES

[1] J. Viefhaus, F. Scholz, S. Deinert, L. Glaser, M. Ilchen, J. Seltmann, P. Walter, and F. Siewert, Nuclear Instruments & Methods In Physics Research A **710**, 151–154 (2013).

[2] E. Allaria, B. Diviacco, C. Callegari, P. Finetti, B. Mahieu, J. Viefhaus, M. Zangrando, G. De Ninno, G. Lambert, E. Ferrari, J. Buck, M. Ilchen, B. Vodungbo, N. Mahne, C. Svetina, C. Spezzani, S. Di Mitri, G. Penco, M. Trovo, W. M. Fawley, P. R. Rebernik, D. Gauthier, C. Grazioli, M. Coreno, B. Ressel, A. Kivimaeki, T. Mazza, L. Glaser, F. Scholz, J. Seltmann, P. Gessler, J. Gruenert, A. De Fanis, M. Meyer, A. Knie, S. P. Moeller, L. Raimondi, F. Capotondi, E. Pedersoli, O. Plekan, M. B. Danailov, A. Demidovich, I. Nikolov, A. Abrami, J. Gautier, J. Luening, P. Zeitoun, and L. Giannessi, Physical Review X **4**, 041040–1–15 (2014).

[3] E. Ferrari, E. Allaria, J. Buck, G. De Ninno, B. Diviacco, D. Gauthier, L. Giannessi, L. Glaser, Z. Huang, M. Ilchen, G. Lambert, A. A. Lutman, B. Mahieu, G. Penco, C. Spezzani, and J. Viefhaus, Scientific Reports **5**, 13531–1–8 (2015).

[4] A. A. Lutman, J. P. MacArthur, M. Ilchen, A. O. Lindahl, J. Buck, R. N. Coffee, G. L. Dakovski, L. Dammann, Y. Ding, H. A. Durr, L. Glaser, J. Grunert, G. Hartmann, N. Hartmann, D. Higley, K. Hirsch, Y. I. Levashov, A. Marinelli, T. Maxwell, A. Mitra, S. Moeller, T. Osipov, F. Peters, M. Planas, I. Shevchuk,

W. F. Schlotter, F. Scholz, J. Seltmann, J. Viefhaus, P. Walter, Z. R. Wolf, Z. Huang, and H.-D. Nuhn, Nature Photonics **10**, 468–472 (2016).

[5] G. Hartmann, A. O. Lindahl, A. Knie, N. Hartmann, A. A. Lutman, J. P. MacArthur, I. Shevchuk, J. Buck, A. Galler, J. M. Glownia, W. Helml, Z. Huang, N. M. Kabachnik, A. K. Kazansky, J. Liu, A. Marinelli, T. Mazza, H. D. Nuhn, P. Walter, J. Viefhaus, M. Meyer, S. Moeller, R. N. Coffee, and M. Ilchen, Review of Scientific Instruments **87**, 083113–1–6 (2016).

[6] C. v. K. Schmising, D. Weder, T. Noll, B. Pfau, M. Hennecke, C. Strueber, I. Radu, M. Schneider, S. Staeck, C. M. Guenther, J. Luning, A. e. D. Merhe, J. Buck, G. Hartmann, J. Viefhaus, R. Treusch, and S. Eisebitt, Review of Scientific Instruments **88**, 053903–1–8 (2017).

[7] L. Mueller, G. Hartmann, S. Schleitzer, M. H. Berntsen, M. Walther, R. Rysov, W. Roseker, F. Scholz, J. Seltmann, L. Glaser, J. Viefhaus, K. Mertens, K. Bagschik, R. Froemter, A. De Fanis, I. Shevchuk, K. Medjanik, G. Oehrwall, H. P. Oepen, M. Martins, M. Meyer, and G. Gruebel, Review of Scientific Instruments **89**, 036103–1–3 (2018).

[8] N. Hartmann, G. Hartmann, R. Heider, M. S. Wagner, M. Ilchen, J. Buck, A. O. Lindahl, C. Benko, J. Gruenert, J. Krzywinski, J. Liu, A. A. Lutman, A. Marinelli, T. Maxwell, A. A. Miahnahri, S. P. Moeller, M. Planas, J. Robinson, A. K. Kazansky, N. M. Kabachnik, J. Viefhaus, T. Feurer, R. Kienberger, R. N. Coffee, and W. Helml, Nature Photonics **12**, 215–220 (2018).

[9] M. Waitz, R. Y. Bello, D. Metz, J. Lower, F. Trinter, C. Schober, M. Keiling, U. Lenz, M. Pitzer, K. Mertens, M. Martins, J. Viefhaus, S. Klumpp, T. Weber, L. P. H. Schmidt, J. B. Williams, M. S. Schoeffler, V. V. Serov, A. S. Kheifets, L. Argenti, A. Palacios, F. Martin, T. Jahnke, and R. Doerner, Nature Communications **8**, 2266–1–8 (2017).

[10] I. T. Jolliffe and J. Cadima, Philosophical Transactions of the Royal Society A **374**, 20150202–1–16 (2016).

[11] J. Buck, J. Viefhaus, F. Scholz, M. Ilchen, L. Glaser, C. Oezkan, W. Freund, J. Gruenert, and S. Molodtsov, *X-ray Free-electron Lasers: Beam Diagnostics, Beamline Instrumentation, and Applications*, Proceedings of SPIE , **8504**, 85040U–1–8 (2012).

[12] M. Braune, J. Buck, M. Kuhlmann, S. Grunewald, S. Düsterer, J. Viefhaus, and K. Tiedtke, Journal of Synchrotron Radiation **25**, 3–15 (2018).